PHYSICAL REVIEW B **77**, 081101(R) (2008)

Visualization of charge ordering in a half-doped manganite by an electrostatic potential analysis

K. Kato
RIKEN SPring-8 Center, 1-1-1 Kouto, Sayo-cho, Sayo-gun, Hyogo 679-5148, Japan

Y. Moritomo
Department of Physics, University of Tsukuba, Tsukuba 305-8571, Japan

M. Takata
RIKEN SPring-8 Center, 1-1-1 Kouto, Sayo-cho, Sayo-gun, Hyogo 679-5148, Japan
and Department of Advanced Materials Science, University of Tokyo, Kashiwa 277-8561, Japan

H. Tanaka
Department of Materials Science, Shimane University, Shimane 690-8504, Japan

N. Hamada
Faculty of Science and Technology, Tokyo University of Science, Noda 278-8510, Japan
(Received 4 January 2008; published 28 February 2008)

We have experimentally investigated the charge density distribution and the electrostatic potential for a charge-ordering doped manganite, $Nd_{1/2}Sr_{1/2}MnO_3$. In the charge-ordered state, we observed a zigzag pattern of the charge density within the (010) plane. Judging from the MnO_6 distortion, we ascribed the pattern to the bonding electron in the $p_{x(y)}-d_{x^2-y^2}$ hybridized state, not to the so-called $d_{3x^2-r^2}/d_{3y^2-r^2}$ orbital ordering. We further calculated the electrostatic potential $U(r)$ from the charge density and the atomic positions, which clearly indicates the checkerboard-type charge disproportionation within the (010) plane.

DOI: 10.1103/PhysRevB.77.081101 PACS number(s): 71.30.+h, 61.05.cp

In the strongly correlated oxide systems, the repulsive interaction between the electrons causes a variety of charge ordering and/or stripe patterns.[1–3] Especially in the so-called doped manganite, the charge ordering couples with the spin and orbital degree of freedoms and causes a variety of spin-charge-orbital ordered states.[4–7] Among them, $Nd_{1/2}Sr_{1/2}MnO_3$ shows a characteristic charge-ordering transition at $T_{CO}=150$ K, which accompanies a significant structural change as well as an antiferromagnetic spin ordering.[8,9] The charge-ordered (CO) phase was believed to be a fully charge separated phase with the Mn^{3+} ions and the Mn^{4+} ions. Nakamura *et al.*[10] investigated the resonant x-ray scattering in $Nd_{1/2}Sr_{1/2}MnO_3$ and analyzed the data with an orbital (or ionic) model. They found that the intensity dependence on the photon energy and on the azimuthal angle is consistent with the $d_{3x^2-r^2}/d_{3y^2-r^2}$ orbital alternation on the Mn^{3+} site. Herrero-Martín *et al.*,[11] however, reconsidered the resonant x-ray scattering experiment in $Nd_{1/2}Sr_{1/2}MnO_3$ by including the distortion of the MnO_6 octahedra. They concluded that even a small charge disproportionation $\Delta(=0.16)$ can explain the experimental data. Their conclusion is further supported by the valence bond sum calculation based on the neutron structural analysis:[12] the deduced $\Delta(=0.15)$ is much less than unity in $Pr_{1/2}Ca_{1/2}MnO_3$. Thus, the electronic state of the CO phase in the half-doped manganites is still controversial.[13,14]

The charge density level structural analysis based on the maximum entropy method (MEM) combined with the Rietveld analysis[15] may give us a clue to comprehend the electronic state of the CO phase. In the MEM-Rietveld method, the observed structural factors are evaluated from the Rietveld refinement of the powder diffraction patterns. Then, a most obscure three-dimensional charge density distribution, which fulfills the observed structural factors within the margin of experimental error, is deduced by the maximum entropy method. Here we emphasize that the accuracy of the structural factors obtained by the synchrotron radiation x-ray powder diffraction pattern is comparable with those obtained by the silicon (diamond) single crystal. The evaluated charge density at the midpoint of the Si-Si (C-C) bond agrees well with the different kinds of theoretical calculations.[16] The MEM-Rietveld method is further applied to the charge density study in several transition metal compounds, e.g., $RbMn[Fe(CN)_6]$[17], $Nd_{0.35}Sr_{0.65}MnO_3$,[18] $La_{1.04}Sr_{1.96}Mn_2O_7$,[19] and $NdSr_2Mn_2O_7$.[20] Especially, the method succeeded in the direct observation of a single electron transfer between the Mn site to the Fe site at the charge-transfer transition of $RbMn[Fe(CN)_6]$. The total charge n at the Mn site, which was estimated from the MEM charge density, decreases from 23.0(2) to 22.2(2), suggesting that the valence state of the Mn ions changes from Mn^{2+} to Mn^{3+}. We emphasize that the MEM charge densities of both the phases are well reproduced by a band calculation with the full-potential linearized augmented plane wave (FLAPW) method[21,22] within the local-density approximation (LDA) scheme.[23–25]

In this Rapid Communication, we have applied the MEM-Rietveld method to a charge-ordering manganite, $Nd_{1/2}Sr_{1/2}MnO_3$. In the CO state, we observed a zigzag pattern of the charge density within the (010) plane, and ascribed the pattern to the bonding electron in the $p-d$ hybridized state. The MEM charge density of the CO phase suggests a finite Δ between the two structurally independent Mn sites. Based on these analyses, we will discuss the elec-

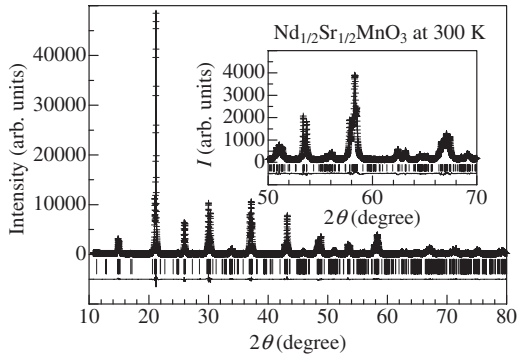

FIG. 1. Rietveld fitting of the x-ray diffraction pattern of $Nd_{1/2}Sr_{1/2}MnO_3$ at 300 K. The solid curve and crosses are the calculated result and the experimental data, respectively. The bars present the calculated reflection positions. The bottom curve is the difference between the calculation and experiment.

tronic state of the CO phase of $Nd_{1/2}Sr_{1/2}MnO_3$.

The electron density distribution of $Nd_{1/2}Sr_{1/2}MnO_3$ was visualized by MEM-Rietveld[15] analysis on the synchrotron radiation (SR) x-ray powder profiles obtained at Photon Factory BL-3A. The detail of the MEM-Rietveld method is described in a previous paper.[15] A single crystal of $Nd_{1/2}Sr_{1/2}MnO_3$, which was grown in a flow of oxygen in a floating-zone furnace at a feeding speed of 7–9 mm/h, was crushed into fine powders. A precipitation method[20] was adopted in order to obtain a fine powder, typically of ~ 3 μm, which gives a homogeneous and sharp intensity distribution in the Debye-Scherrer powder ring. The powders were filled into a flat plate type glass (copper) holder at 300 K (18 K). The homogeneity and the sharpness are necessary conditions for a reliable MEM-Rietveld analysis. The wavelength of the incident x ray is about 1.0 Å. The collection time at each step of 2θ (=0.01°) was 20.0 s. The data range in 2θ was from 10.69° to 80.69° (9.99° to 75.49°) at 300 K (18 K). The atomic positions and the observed structural factors were refined by the Rietveld analysis with the *Imma* (Z=4) space group for the charge-disordered phase at 300 K. For the CO phase at 18 K, the *Pmmn* (Z=8) space group is adopted. As an example, we show in Fig. 1 the result of the Rietveld refinement at 300 K. We show in Table I and Table II the atomic coordinates refined by the Rietveld analysis for $Nd_{1/2}Sr_{1/2}MnO_3$ at 300 K and 18 K, respectively. The MEM analysis was carried out with the program

TABLE I. Atomic coordinates, isotropic atomic displacement parameters B, and occupancy g for $Nd_{1/2}Sr_{1/2}MnO_3$ at 300 K. The space group is *Imma* (Z=4). Lattice constant is a=5.427 28(4) Å, b=7.626 64(4) Å, and c=5.472 54(4) Å. R_{wp} and R_I are 5.9% and 2.5%, respectively.

Atom	Site	g	x	y	z	B (Å^2)
Nd/Sr	4*e*	1	0	1/4	0.0020(2)	0.357(7)
Mn	4*b*	1	0	0	1/2	0.18(1)
O1	4*e*	1	0	1/4	0.5497(8)	0.6(1)
O2	8*g*	1	1/4	0.0263(4)	1/4	1.19(7)

TABLE II. Atomic coordinates, isotropic atomic displacement parameters B, and occupancy g for $Nd_{1/2}Sr_{1/2}MnO_3$ at 18 K. The space group is *Pmmn* (Z=8). The lattice constant is a=10.877 91(9) Å, b=7.517 33(4) Å, and c=5.508 79(4) Å. R_{wp} and R_I are 7.8% and 4.0%, respectively.

Atom	Site	g	x	y	z	B (Å^2)
Nd1/Sr1	4*f*	1	0.0	1/4	0.49816	0.167(8)
Nd2/Sr2	2*a*	1	1/4	1/4	−0.0131(3)	0.167(8)
Nd3/Sr3	2*b*	1	1/4	3/4	0.9832(3)	0.167(8)
Mn1	4*c*	1	0	0	0	0.1
Mn2	4*e*	1	1/4	0.0	0.4868(6)	0.1
O1	4*f*	1	0.0	1/4	0.94098	0.8(1)
O2	2*a*	1	1/4	1/4	0.5458(6)	0.8(1)
O3	2*b*	1	1/4	3/4	0.4277(6)	0.8(1)
O4	8*g*	1	0.125	0.02778	0.2368(6)	0.90(7)
O5	8*g*	1	0.125	0.97222	0.7368(6)	0.90(7)

ENIGMA[26] using $64\times128\times64$ pixels ($128\times128\times64$) at 300 K (18 K) on the structural factors derived by the Rietveld analysis. The number of the structural factors derived by the Rietveld analysis were 133 (466) at 300 K (at 18 K): the maximum (minimum) d values were 4.45 Å (0.82 Å) at 300 K and 5.51 Å (0.82 Å) at 18 K. The R_F factor based on the MEM charge densities is 1.2% (2.3%) at 300 K (18 K).

Figure 2 shows the contour map of the MEM charge density distribution of $Nd_{1/2}Sr_{1/2}MnO_3$ for the (010) plane in [Fig. 2(a)] the charge-disordered phase and [Fig. 2(b)] the CO phase. In the charge-disordered phase [Fig. 2(a)] all the Mn sites are crystallographically equivalent and the charge density around the Mn site are isotropic. The charge density (=0.68e Å^{-3}) at the center of the Mn-O bond may be ascribed to the itinerant e_g electrons. In the CO phase [Fig. 2(b)], however, the neighboring Mn sites, i.e., Mn1 and Mn2, become nonequivalent. The charge density within the Mn1-O4 bond is much higher, showing a zigzag charge density pattern along the (100) direction. The charge density at the center of the Mn1-O4 (Mn1-O5) bond is 1.01e Å^{-3} (0.63e Å^{-3}). At a glance, this zigzag chain looks similar to the $d_{3x^2-r^2}/d_{3y^2-r^2}$ orbital-ordering pattern proposed by the resonance x-ray scattering experiment.[10] This simple orbital picture has to be abandoned due to the following reason. In the CO phase, the $Mn1O_6$ octahedron shows a Jahn-Teller-type (2-long/4-short type) distortion within the (010) plane; the Mn1-O4 (Mn1-O5) bond distance is 1.896(3) Å [1.999(3) Å]. That is, the charge density within the Mn1-O bond is higher for the shorter bond. This observation contradicts with a simple orbital picture, which predicts that the extra electron tends to occupies the e_g orbital that extends along the longer bond.

In order to comprehend the observed zigzag pattern, we have to include the $p-d$ hybridization effect. Kato *et al.*[17] have investigated the charge density distribution around the Mn^{3+} site of $RbMn[Fe(CN)_6]$. They found that the charge density at the center of the Mn^{3+}-N bond is higher along the shorter bond. Based on the LDA band calculation, they concluded that the charge density on the shorter Mn^{3+}-N bond is

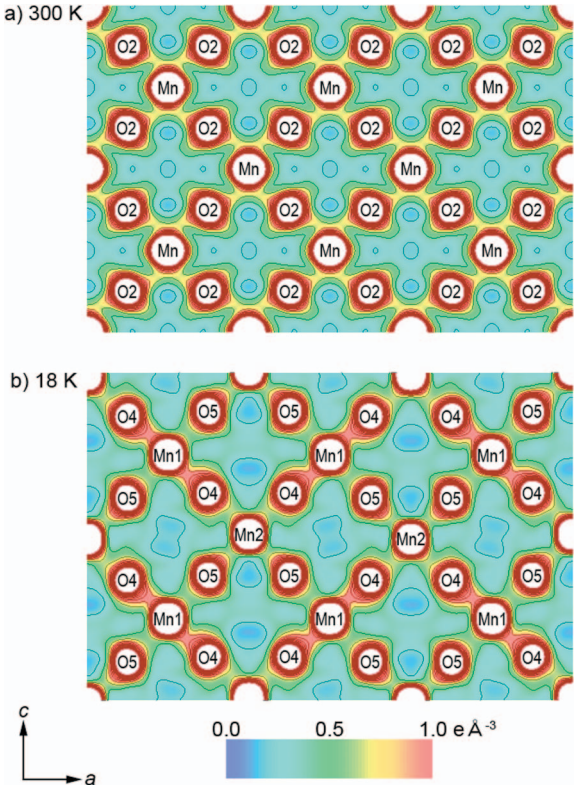

FIG. 2. (Color) Contour map of the MEM electron density distribution of $Nd_{1/2}Sr_{1/2}MnO_3$ for the (010) plane at (a) 300 K and (b) 18 K. Contour lines are drawn from $0.0e$ Å^{-3} to $4.0e$ Å^{-3} at intervals of $0.2e$ Å^{-3}.

due to the $p_{x(y)}-d_{x^2-y^2}$ hybridization. We think that a similar scenario is applicable to the present $Nd_{1/2}Sr_{1/2}MnO_3$ system. We have investigated the effect of the $p-d$ hybridization on charge density distribution in a cubic $La_{1/2}Ba_{1/2}MnO_3$ virtual crystal, in which the Mn-O bond distance alternates at a rate of 1.04:0.96. We have performed a band calculation with the FLAPW method within the LDA+U scheme (U=2 eV).[27,28] Consistent with the experiment, the charge density is higher in the shorter Mn-O bond due to the $p_{x(y)}-d_{x^2-y^2}$ hybridization.

Now, let us proceed to the total charge n at the Mn site. We have evaluated the n value by the spherical integration, and plotted them against the radius r of the sphere in Fig. 3. In both the phases, the magnitude of n monotonously increases with r, suggesting that the wave functions of the electrons extend around the Mn site reflecting the strong $p-d$ hybridization. Here, we confirm that the n value evaluated from the MEM charge density has some ambiguity, especially when the bonding electrons have high charge density. If we set r at the midpoint of the Mn-O bond, n is estimated to be $21.3(2)e$ [$20.0(2)e$] for the Mn1 (Mn2) site at 18 K and $21.0(2)e$ for the Mn site at 300 K. The total charge [$=21.0(2)e$] in the charge-disordered phase at 300 K is much less than the nominal one [$=22.5e$ for the $Mn^{3.5+}$ state]. This is probably due to the strong $p-d$ hybridization and resultant extension of the wave functions. Nevertheless, the parallel increase of the total charges at the Mn1 site and the Mn2 site suggests that there exists a finite charge disproportionation in the CO phase.

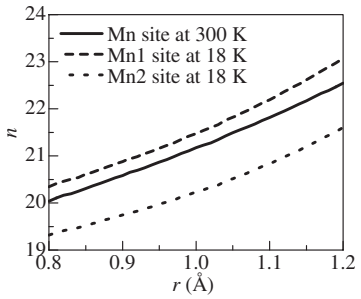

FIG. 3. Total charge n at the Mn sites of $Nd_{1/2}Sr_{1/2}MnO_3$. n was evaluated by the spherical integration of the MEM charge density up to the radius r.

It may be interesting to compare the charge disproportionation Δ with the value estimated by the valence bond method.[29] The effective Mn valences estimated from the Mn-O bond distances are +3.57 at 300 K and +3.50 (+3.66) at the Mn1 (Mn2) site. The Δ value ($\sim$1) estimated from the MEM charge density is much larger than the value (=0.16) estimated by the valence bond method. The valence bond method empirically includes the effects of the surrounding ligands on the valence state of central metal ions. Then, the enhancement of Δ should be ascribed to the nearest-neighbor electron repulsion V, which is not included in the "classical" analysis. Here we stress that a simple ionic picture does not properly describe the electronic state of the

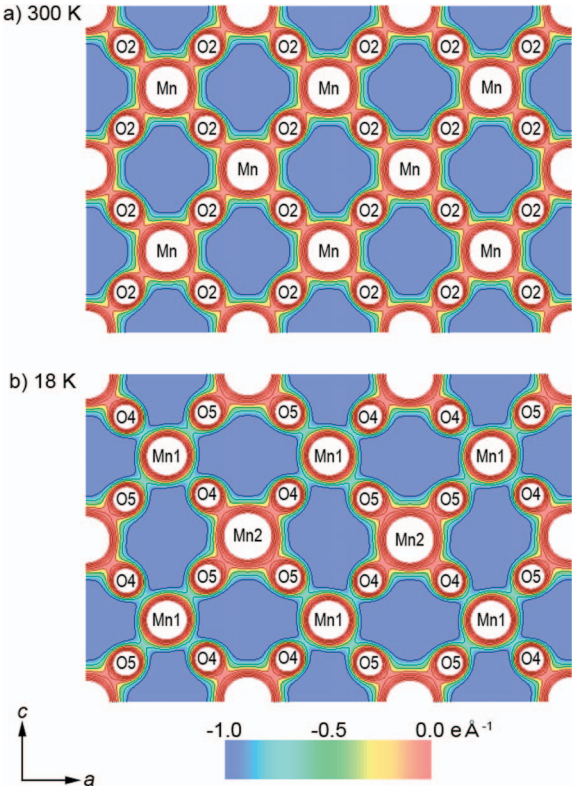

FIG. 4. (Color) Contour map of the electrostatic potential $U(r)$ of $Nd_{1/2}Sr_{1/2}MnO_3$ for the (010) plane at (a) 300 K and (b) 18 K. Contour lines are drawn from $-1.0e$ Å^{-1} to $2.0e$ Å^{-1} at intervals of $0.3e$ Å^{-1}.

CO phase because the charge density around the Mn1 site is dominated by the bonding electrons, not the isolated e_g electrons (see Fig. 2). In addition, the wave functions around the Mn site extend significantly, as seen in Fig. 3. The MEM charge density suggests that the $p-d$ hybridization is the key to comprehend the electronic state of the CO phase.

Finally, let us investigate the electrostatic potential $U(r)$ according to Tanaka's procedure,[30] in which $U(r)$ is divided into the nucleus charge component $[U_n(r)]$ and the electron charge component $[U_e(r)]$. The magnitude of $U_n(r)$ is estimated by the ordinary Ewald's method with use of the atomic positions listed in Table I and Table II, while $U_e(r)$ is directly calculated from the MEM charge density in the reciprocal space. Figure 4 shows the contour map of $U(r)$ of $Nd_{1/2}Sr_{1/2}MnO_3$ for the (010) plane in [Fig. 4(a)] the charge-disordered phase and [Fig. 4(b)] the CO phase. In the charge-disordered phase [Fig. 4(a)], all the Mn sites are crystallographically equivalent. In the CO phase [Fig. 4(b)], the charge disproportionation significantly modifies the profile of $U(r)$. The magnitude of $U(r)$ around the Mn1 site is suppressed, while that around the Mn2 site is enhanced. This is because the added (subtracted) charge density at the Mn1 (Mn2) site enhances (weakens) the screening of the positive nucleus charge. Thus, the electrostatic potential $U(r)$ clearly indicates the checkerboard-type charge disproportionation within the (010) plane.

In conclusion, we have experimentally investigated the charge density distribution and the electrostatic potential for a charge-ordering manganite $Nd_{1/2}Sr_{1/2}MnO_3$. The total charge n estimated by the spherical integration of the MEM charge density suggests a finite Δ in the CO phase, which is probably ascribed to the nearest-neighbor electron repulsion V. The contour map of $U(r)$ is a powerful tool to visualize the charge disproportionation of the transition metal compounds.

This work was supported by a Grant-In-Aid for Scientific Research from the Ministry of Education, Culture, Sports, Science and Technology. The synchrotron-radiation x-ray powder diffraction experiments were performed at Photon Factory BL-3A. The authors thank E. Nishibori and M. Sakata for their help in the synchrotron radiation experiment and MEM/Rietveld analysis.

[1] J. M. Tranquada, B. J. Sternlieb, J. D. Axe, Y. Nakamura, and S. Uchida, Nature (London) **375**, 561 (1995).
[2] S. Mori, C. H. Chen, and S.-W. Cheong, Nature (London) **392**, 473 (1998).
[3] Y. Murakami, H. Kawada, H. Kawata, M. Tanaka, T. Arima, Y. Moritomo, and Y. Tokura, Phys. Rev. Lett. **80**, 1932 (1998).
[4] Y. Tokura and N. Nagaosa, Science **288**, 462 (2000).
[5] R. Maezono, S. Ishihara, and N. Nagaosa, Phys. Rev. B **58**, 11583 (1998).
[6] R. Maezono and N. Nagaosa, Phys. Rev. B **61**, 1825 (2000).
[7] J. vandenBrink and D. Khomskii, Phys. Rev. Lett. **82**, 1016 (1999).
[8] R. Kajimoto, H. Yoshizawa, H. Kawano, H. Kuwahara, Y. Tokura, K. Ohoyama, and M. Ohashi, Phys. Rev. B **60**, 9506 (1999).
[9] H. Kawano, R. Kajimoto, H. Yoshizawa, Y. Tomioka, H. Kuwahara, and Y. Tokura, Phys. Rev. Lett. **78**, 4253 (1997).
[10] K. Nakamura, T. Arima, A. Nakazawa, Y. Wakabayashi, and Y. Murakami, Phys. Rev. B **60**, 2425 (1999).
[11] J. Herrero-Martín, J. García, G. Subías, J. Blasco, and C. Sánchez, Phys. Rev. B **70**, 024408 (2004).
[12] R. J. Goff and J. P. Attfield, Phys. Rev. B **70**, 140404(R) (2004).
[13] M. v. Zimmermann, C. S. Nelson, J. P. Hill, D. Gibbs, M. Blume, D. Casa, B. Keimer, Y. Murakami, C.-C. Kao, C. Venkataraman, T. Gog, Y. Tomioka, and Y. Tokura, Phys. Rev. B **64**, 195133 (2001); M. v. Zimmermann *et al.*, *ibid.* **68**, 127102 (2003); M. v. Zimmermann *et al.*, *ibid.* **64**, 195133 (2001).
[14] S. Grenier, J. P. Hill, D. Gibbs, K. J. Thomas, M. v. Zimmermann, C. S. Nelson, V. Kiryukhin, Y. Tokura, Y. Tomioka, D. Casa, T. Gog, and C. Venkataraman, Phys. Rev. B **69**, 134419 (2004).
[15] M. Takata, E. Nishibori, and M. Sakata, Z. Kristallogr. **216**, 71 (2001).
[16] E. Nishibori, E. Sunayoshi, A. Yoshida, S. Aoyagi, K. Kato, M. Takata, and M. Sakata, Acta Crystallogr., Sect. A: Found. Crystallogr. **63**, 43 (2007).
[17] K. Kato, Y. Moritomo, M. Takata, M. Sakata, M. Umekawa, N. Hamada, S. Ohkoshi, H. Tokoro, and K. Hashimoto, Phys. Rev. Lett. **91**, 255502 (2003).
[18] K. Kato, M. Takata, E. Nishibori, M. Sakata, N. Hamada, and Y. Moritomo, J. Phys. Soc. Jpn. **74**, 2137 (2005).
[19] K. Kato, Y. Ohishi, M. Takata, E. Nishibori, M. Sakata, and Y. Moritomo, Phys. Rev. B **71**, 012404 (2005).
[20] M. Takata, E. Nishibori, K. Kato, M. Sakata, and Y. Moritomo, J. Phys. Soc. Jpn. **68**, 2190 (1999).
[21] O. K. Andersen, Phys. Rev. B **12**, 3060 (1975).
[22] T. Takeda and J. Kubler, J. Phys. F: Met. Phys. **9**, 661 (1979).
[23] P. Hohenberg and W. Kohn, Phys. Rev. **136**, B864 (1964).
[24] W. Kohn and L. J. Sham, Phys. Rev. **140**, A1133 (1965).
[25] S. H. Vosko, L. Wilk, and M. Nusair, Can. J. Phys. **58**, 1200 (1980).
[26] H. Tanaka, M. Takata, E. Nishibori, K. Kato, T. Iishi, and M. Sakata, J. Appl. Crystallogr. **35**, 282 (2002).
[27] V. I. Anisimov, I. V. Solovyev, M. A. Korotin, M. T. Czyzyk, and G. A. Sawatzky, Phys. Rev. B **48**, 16929 (1993).
[28] I. V. Solovyev, P. H. Dederichs, and V. I. Anisimov, Phys. Rev. B **50**, 16861 (1994).
[29] I. D. Brown and D. Altermatt, Acta Crystallogr., Sect. B: Struct. Sci. **41**, 244 (1985).
[30] H. Tanaka, Y. Kuroiwa, and M. Takata, Phys. Rev. B **74**, 172105 (2006).